JOURNAL OF GEOPHYSICAL RESEARCH, VOL. 113, C07025, doi:10.1029/2007JC004514, 2008

Wave-driven setup and alongshore flows observed onshore of a submarine canyon

Alex Apotsos,[1] Britt Raubenheimer,[1] Steve Elgar,[1] and R. T. Guza[2]

Received 20 August 2007; revised 12 December 2007; accepted 17 March 2008; published 19 July 2008.

[1] The effect of alongshore variations in the incident wavefield on wave-driven setup and on alongshore flows in the surfzone is investigated using observations collected onshore of a submarine canyon. Wave heights and radiation stresses at the outer edge of the surfzone (water depth ≈2.5 m) varied by up to a factor of 4 and 16, respectively, over a 450 m alongshore distance, resulting in setup variations as large as 0.1 m along the shoreline (water depth ≈0.3 m). Even with this strong alongshore variability, wave-driven setup was dominated by the cross-shore gradient of the wave radiation stress, and setup observed in the surfzone is predicted well by a one-dimensional cross-shore momentum balance. Both cross-shore radiation stress gradients and alongshore setup gradients contributed to the alongshore flows observed in the inner surfzone when alongshore gradients in offshore wave heights were large, and a simplified alongshore momentum balance suggests that the large [O(1 kg/(s^2 m)] observed setup-induced pressure gradients can drive strong [O(1 m/s)] alongshore currents.

Citation: Apotsos, A., B. Raubenheimer, S. Elgar, and R. T. Guza (2008), Wave-driven setup and alongshore flows observed onshore of a submarine canyon, *J. Geophys. Res.*, *113*, C07025, doi:10.1029/2007JC004514.

1. Introduction

[2] Setup, the increase in the mean sea level owing to breaking waves, and alongshore flows are predicted well by one-dimensional (1-D) momentum balances on coasts that are roughly alongshore uniform [*Battjes and Stive*, 1985; *Feddersen et al.*, 1998, 2004; *Lentz and Raubenheimer*, 1999; *Raubenheimer et al.*, 2001; *Ruessink et al.*, 2001; *Reniers et al.*, 2002; *Van Dongeren et al.*, 2003; *Apotsos et al.*, 2006, 2007]. However, large alongshore variations in the surfzone bathymetry can result in setup variations in large enough to drive alongshore-variable currents [*Putrevu et al.*, 1995; *Slinn et al.*, 2000; *Haller et al.*, 2002; *Chen et al.*, 2003; *Haas et al.*, 2003; *Schmidt et al.*, 2005]. Previous studies also have shown that nearshore circulation, including the locations of rip currents, can be controlled by nonuniformities in the offshore (i.e., outside the surfzone) bathymetry [*Long and Özkan-Haller*, 2005]. Here, the effect of strong alongshore variations in the incident wavefield (caused by an offshore submarine canyon [*Long and Özkan-Haller*, 2005; *Magne et al.*, 2007; *Thomson et al.*, 2007]) on setup and on alongshore flows in the surfzone is examined using field observations and simplified one- and two-dimensional momentum balances. After the theories are outlined (section 2) and the observations are described (section 3), the results are presented (section 4) and conclusions are given (section 5).

2. Theory

2.1. Setup: Cross-Shore Momentum Balance

[3] The cross-shore pressure gradient associated with the time-averaged wave setup, $\bar{\eta}$, theoretically balances the sum of the cross- and alongshore gradients of the wave radiation stresses (S_{xx} and S_{xy}) and the bottom stress τ_b [*Longuet-Higgins and Stewart*, 1962, 1964; *Mei*, 1989; *Haller et al.*, 2002], such that

$$-\rho g h \frac{\partial}{\partial x}\bar{\eta} = \frac{\partial}{\partial x}S_{xx} + \frac{\partial}{\partial y}S_{xy} + \tau_b, \tag{1}$$

where ρ is the water density, g is the gravitational acceleration, h is the total water depth (including setup), x is the cross-shore coordinate (positive onshore), and y is the alongshore coordinate (positive to the north). The radiation stress components can be estimated as [*Longuet-Higgins and Stewart*, 1962, 1964; *Svendsen*, 1984a, 1984b]

$$S_{xx} = E_w\left[\left(\cos^2\theta + 1\right)\frac{c_g}{c} - \frac{1}{2}\right] + 2E_r\left(\cos^2\theta\right), \tag{2}$$

and [*Longuet-Higgins*, 1970; *Reniers and Battjes*, 1997; *Ruessink et al.*, 2001]

$$S_{xy} = E_w \cos\theta \sin\theta \frac{c_g}{c} + 2E_r \cos\theta \sin\theta, \tag{3}$$

[1] Woods Hole Oceanographic Institution, Applied Ocean Physics and Engineering, Woods Hole, Massachusetts, USA.
[2] Scripps Institution of Oceanography, Integrative Oceanography Division, University of California at San Diego, La Jolla, California, USA.

0148-0227/08/2007JC004514$09.00

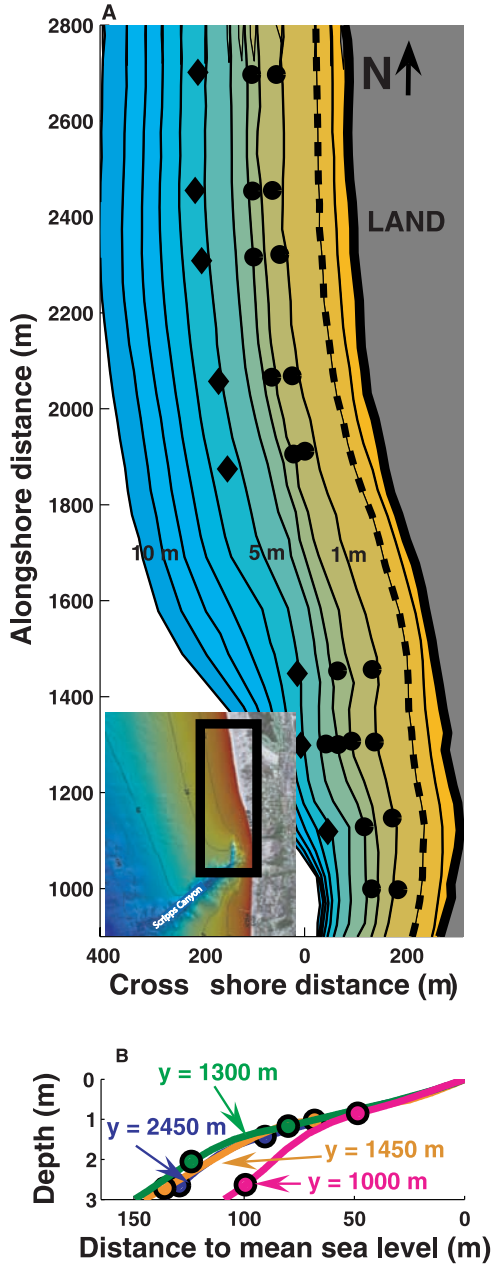

Figure 1. (A) Map of the sensor array (the inset in the lower left corner shows the location (black rectangle) of the array map relative to Scripps submarine canyon). Current meters were colocated with buried (circles) and unburied (diamonds) pressure sensors. Bathymetry near the array is shown by isobaths in 1.0-m intervals (black curves) from 2 m above (darkest yellow) to 10 m below (darkest blue) mean sea level (MSL) (dashed curve). Color scale for bathymetry in the inset ranges from 0 (red) to 300 (darkest blue) m depth. (B) Water depth (curves) and sensor locations (circles) versus the cross-shore distance to the MSL isobath for alongshore distances y = 2450 m (blue), y = 1450 m (orange), y = 1300 m (green), and y = 1000 m (magenta).

where the two terms on the right-hand sides of (2) and (3) are the contributions from the wave and the roller, respectively. Here, θ is the mean wave direction relative to shore normal, c_g and c are the linear group and phase speeds, respectively, and E_w, the linear-theory-derived wave energy, is $E_w = 1/8(\rho g H_{rms}^2)$, where H_{rms} is the root-mean square wave height. The wave roller energy E_r is estimated as [*Stive and De Vriend*, 1994; *Reniers and Battjes*, 1997; *Ruessink et al.*, 2001]

$$\frac{\partial}{\partial x}(2E_r c\cos\theta) = -\frac{2gE_r\sin(\beta)}{c} + D_{br}, \tag{4}$$

where β, the front slope of the wave, is held constant at 0.1, and the wave dissipation D_{br} is

$$D_{br} = -\frac{\partial}{\partial x}(E_w c_g\cos\theta). \tag{5}$$

[4] The bottom stress, τ_b, is estimated using a combined eddy viscosity-undertow model [*Apotsos et al.*, 2007].

[5] As in prior studies [e.g., *Apotsos et al.*, 2006, 2007], contributions to setup owing to broad wave directional spreads, wind stresses, and convective accelerations of the current usually are small and are neglected here.

2.2. Alongshore Flows: Alongshore Momentum Balance

[6] A simplified alongshore momentum balance for the surfzone that includes bottom stress estimated with a quadratic bottom friction formulation $\tau_b = \rho c_d\langle|\vec{u}|v\rangle$ [*Feddersen et al.*, 1998, 2004; *Ruessink et al.*, 2001], the alongshore pressure gradient owing to variations in setup $(\rho g h)\partial\bar{\eta}/\partial y$, and gradients in the wave radiation stresses S_{xy} and S_{yy} [*Mei*, 1989] is given by

$$-\rho c_d\langle|\vec{u}|v\rangle = \rho g h\frac{\partial}{\partial y}\bar{\eta} + \frac{\partial}{\partial x}S_{xy} + \frac{\partial}{\partial y}S_{yy}, \tag{6}$$

where c_d is an empirical drag coefficient, $|\vec{u}|$ is the magnitude of the total instantaneous velocity, v is the instantaneous velocity in the alongshore direction, and $\langle\rangle$ represents time-averaging. The radiation stress component S_{yy} can be estimated as [*Longuet-Higgins and Stewart*, 1962, 1964]

$$S_{yy} = E_w\left[(\sin^2\theta + 1)\frac{c_g}{c} - \frac{1}{2}\right]. \tag{7}$$

[7] For the observations considered here, $\partial S_{yy}/\partial y$ is small relative to the other forcing terms in (6) (see section 4.2.1), and thus (7) is not extended to include the wave roller.

[8] The neglect of wind stress (winds were weak), nonlinear advective terms [*Lentz et al.*, 1999] (which may be important near rip currents [*Haller et al.*, 2002]), mixing [*Özkan-Haller and Kirby*, 1999], and other possible contributions to the alongshore momentum balance does not affect the conclusions (below) that setup can be predicted by a 1-D momentum balance and that alongshore pressure gradients can be important to alongshore flows.

3. Observations

3.1. Measurements

[9] Wave-induced pressures and velocities were measured at 28 locations between the 5.0-m isobath and the shoreline

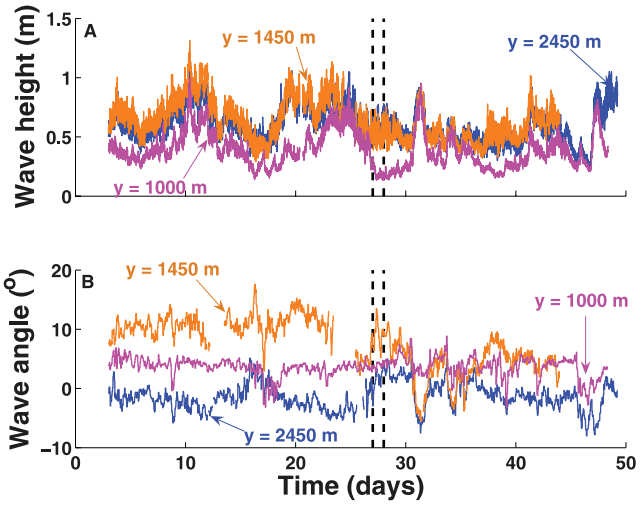

Figure 2. Observed (A) wave height, H_{rms}, and (B) mean wave angle, θ, relative to shore normal versus time (days after 0:00 1 October 2003 PST) on the 2.5-m isobath at y = 2450 m (blue curves), y = 1450 m (orange curves), and y = 1000 m (magenta curves). Positive angles ($\theta > 0$ in B) correspond to waves from the south. The vertical dashed lines bracket 27 October.

along approximately 2 km of coast for 48 d during October and November 2003 near La Jolla, CA just onshore of a deep submarine canyon (Figure 1) [*Thomson et al.*, 2006, 2007]. Sensors were sampled at 2 or 16 Hz for 3072 s (51.2 min) starting every hour. Unless noted otherwise, the 1-h-long data records were subdivided into 8.5-min-long sections, reducing nonstationarity associated with tidally induced depth changes.

[10] The bathymetry between about 10-m water depth and the shoreline was surveyed with roughly 25- to 50-m alongshore spacing approximately weekly using a GPS and altimeter mounted on a personal watercraft. The bathymetry was smoothed by averaging the measured depths over 10-m long sections of each cross-shore profile, and by interpolating the resulting smoothed profiles to 1.0-m grid spacing. For $h < 10$ m, the water depth decreases monotonically toward shore, with an increase in the beach slope near the southern end of the instrumented region (Figure 1b).

[11] Eighteen pressure sensors were buried on about the 1.0- and 2.5-m isobaths at 9 alongshore locations (Figure 1a, roughly y = 2700, 2450, 2321, 2069, 1911, 1450, 1300, 1149, and 1000 m, respectively). Two pressure sensors were buried on approximately the 3.0- and 3.5-m isobaths at y = 1300 m. Eight additional pressure sensors were deployed about 0.5 m above the bed along approximately the 5.0-m isobath at 8 of the alongshore locations. A current meter, deployed between 0.2 and 1.0 m above the bed, was colocated with each pressure sensor.

[12] Root-mean square wave heights, H_{rms}, at each sensor were estimated as $2\sqrt{2}$ times the standard deviation of the sea-surface elevation fluctuations calculated from the time series of pressure (band pass filtered between 0.05 and 0.30 Hz) using linear wave theory and exponential decay of wave fluctuations through the bed [*Raubenheimer et al.*, 1998]. Mean incident wave angles relative to local shore normal (estimated from the 1.0- and 2.5-m isobaths) were calculated from the colocated pressure and velocity observations [*Kuik et al.*, 1988; *Herbers and Guza*, 1990; *Elgar et al.*, 1994]. Owing to the slight curvature of the coast, the orientation of shore normal varied over a 13° range. Mean water levels were estimated at all 20 buried pressure sensors assuming hydrostatic pressure. Drifts and offsets in the estimated mean water levels were removed by assuming the sea surface was flat throughout the instrumented region during nine 8.5-min periods (spaced approximately equally over the 48-d-long deployment) when waves were small at high tide. Corrections to the data were less than 0.02 m. Setup was defined as the increase in the water level relative to that measured on the 3.5-m isobath at y = 1300 m.

[13] Along the 2.5-m isobath, H_{rms} ranged from 0.16 to 1.52 m, and varied by up to a factor of 4 over a 450-m

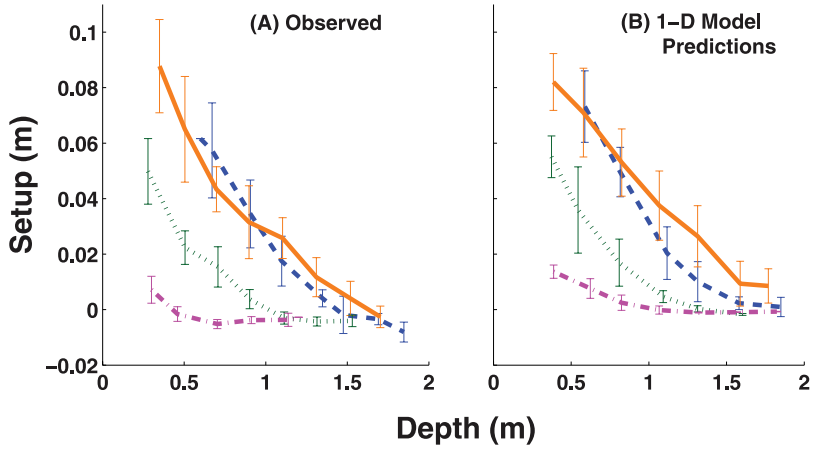

Figure 3. Means (curves) and standard deviations (vertical bars) of 144 (8.5 min) (A) observations and (B) 1-D model predictions of setup at the sensors along the 1.0-m isobath from 0:00 to 23:42 27 October 2003 in 0.2-m-wide depth bins versus water depth at y = 2450 m (dashed blue curve), y = 1450 m (solid orange curve), y = 1300 m (dotted green curve), and y = 1000 m (dashed-dotted magenta curve). On 27 October the mean and standard deviation of H_{rms} on the 2.5-m isobath at y = 1450 m were 0.53 m and 0.07 m, respectively, and the tidal range was −0.92 to 1.35 m relative to MSL.

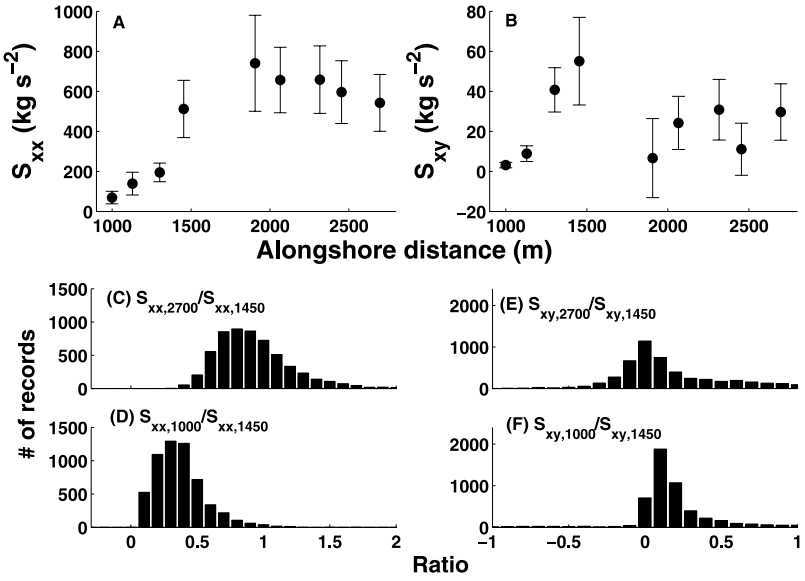

Figure 4. (A) S_{xx} and (B) S_{xy} estimated at the sensors on the 2.5-m isobath for the 144 8.5-min-long data records on 27 October 2003 (filled circles show means, and bars show one standard deviation). Histograms of the ratios of S_{xx} at (C) y = 2700 m and (D) y = 1000 m to S_{xx} at y = 1450 m, and of S_{xy} at (E) y = 2700 m and (F) y = 1000 m to S_{xy} at y = 1450 m for all data records. Negative ratios of S_{xy} (E & F) result when waves along different cross-shore transects approach the shoreline from opposite sides of shore normal.

alongshore distance onshore of the canyon head (Figure 2a, compare the orange with the magenta curve). Centroidal frequencies (f_c, the frequency corresponding to the centroid of the sea-surface elevation spectrum between 0.05 and 0.30 Hz) along the 2.5-m isobath ranged from 0.07 to 0.19 Hz. Although incident waves were within 5° of local shore normal along most cross-shore transects (Figure 2b, blue and magenta curves), wave angles of 10° to 15° were observed near the canyon head [e.g., at y = 1450 m (Figure 2b, orange curve) and 1300 m]. Setup ranged from −0.02 m to 0.20 m, and the tide ranged from −0.96 to 1.36 m relative to mean sea level (MSL).

[14] Data from 27 October 2003, a day with constant wave conditions and large alongshore wave height gradients near the canyon head (H_{rms} = 0.53 m at y = 1450 m was approximately 3 times larger than H_{rms} at y = 1000 m), were used to generate 24-h average curves of $\bar{\eta}$ versus water depth (Figure 3a). Comparisons of the curves for each cross-shore transect show that setup varied in the alongshore by as much as 0.10 m (Figure 3a).

3.2. Estimates of S_{xx}, S_{xy}, and S_{yy}

[15] The radiation stress tensor components (S_{xx}, S_{xy}, and S_{yy}) were estimated relative to local shore normal at each sensor location with (2), (3), and (7), respectively, using H_{rms} and θ estimated from the observations, and c_g and c estimated with linear theory using f_c and h. The results are not sensitive to the method used to estimate the momentum fluxes [*Ruessink et al.*, 2001; *Feddersen*, 2004], possibly owing to the relatively narrow directional distributions of the incident wavefield. For observation-based estimates of S_{xx} and S_{xy} the effects of the roller, which shifts the forcing in the cross-shore, are not resolved and therefore are neglected [i.e., E_r = 0 in both (2) and (3)]. Roller effects are included in all numerical model predictions.

[16] Estimates of S_{xx} (Figures 4a, c, d) and S_{yy} (not shown) were nearly uniform (i.e., 80% of the estimates were within approximately 30% of each other) north of the canyon head (y > 1400 m, Figures 4a and 4c). However, near and south of the canyon head (1000 < y < 1400 m) estimates of S_{xx} and S_{yy} usually were 60% smaller (and as much as 85% smaller) than those farther north (Figures 4a and 4d, compare estimates at y = 1000 m with those at y = 1450 m).

[17] Owing to the small wave angles observed along most transects (Figure 2b, blue and magenta curves), S_{xy} was small at most locations. However, at y = 1450 and 1300 m, where θ often was 10° or more (e.g., Figure 2b, orange curve), S_{xy} was as much as a factor of 16 larger than S_{xy} estimated elsewhere, and usually was at least twice as large as estimates at y = 1000 and 2700 m (Figures 4b, 4e, and 4f).

4. Results

4.1. Setup: Cross-Shore Momentum Balance

[18] The effect of alongshore variations in the incident wavefield on wave-driven setup is determined using a numerical model based on (1). The model is initialized with h, H_{rms}, $\bar{\eta}$, and θ measured at the location of the 2.5-m isobath sensors along each cross-shore transect. A wave transformation model [*Thornton and Guza*, 1983; *Apotsos et al.*, 2008] is used to predict wave heights along each shore-normal instrumented transect using a 1-m cross-shore grid step. Comparisons with observations on the 1.0-m isobath suggest that errors in predicted wave heights are less than 0.06 m. Wave angles are refracted shoreward using Snell's Law, and c_g and c are estimated from h (including the predicted setup) and f_c (assumed constant along each transect). At each grid point, E_r is determined from (4) and (5), and S_{xx} and S_{xy} are determined from (2) and (3), respectively. The forcing $\partial S_{xx}/\partial x$ is estimated by finite

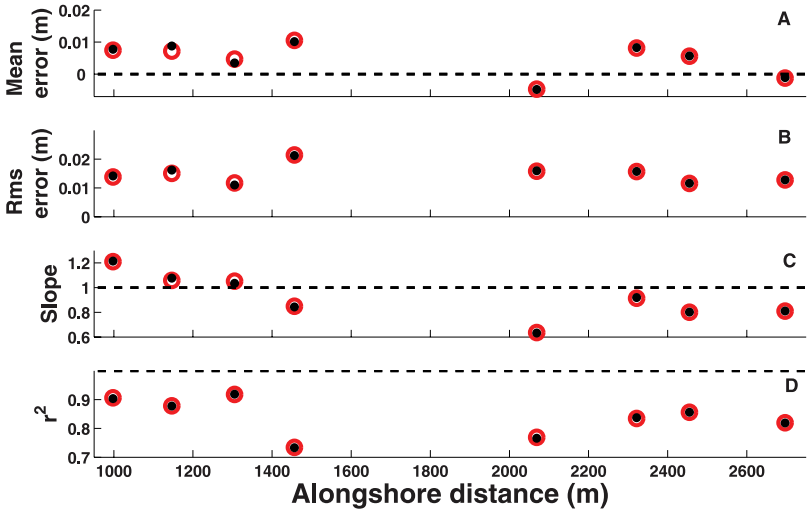

Figure 5. (A) Mean and (B) root-mean square (RMS) errors, (C) best fit linear slopes, and (D) squared correlations between the observations and predictions of setup in $0.3 < h < 1.0$ m for a model based on (1) (solid black circles) and for a 1-D model [i.e., $\partial S_{xy}/\partial y = 0$ in (1)] (open red circles) versus alongshore distance for all data records. Data are not shown at $y = 1911$ m because the small cross-shore separation between the sensors on the 2.5- and 1.0-m isobaths results in relatively small changes in setup between the two sensors.

differencing estimates of S_{xx} at successive cross-shore grid points. Values of S_{xy} from neighboring transects are used to estimate $\partial S_{xy}/\partial y$ along the appropriate isobath at each cross-shore grid point using central differencing (see Appendix). The modeled setup is calculated by integrating (1) shoreward along each transect for every data record.

[19] At all alongshore locations, the observed and modeled setup are correlated ($r^2 > 0.7$), with regression slopes usually within 1.0 ± 0.2 (Figure 5, solid black circles). Model errors are similar to those found on alongshore-homogeneous beaches [e.g., *Apotsos et al.*, 2006, 2007] (Figure 5), and may be owing to physics neglected in the simple momentum balance (1) [see *Apotsos et al.*, 2007], to errors in the predicted waves [*Apotsos et al.*, 2008], or to errors in the radiation stress estimates and bathymetric measurements.

[20] Simple scaling arguments (e.g., $S_{xy} \ll S_{xx}$, $\partial y \geq \partial x$) and observation-based estimates (see Appendix) suggest that $\partial S_{xy}/\partial y \ll \partial S_{xx}/\partial x$. Neglecting $\partial S_{xy}/\partial y$ in (1) changes the predicted setup for $0.3 < h < 1.0$ m by less than 5% (Figure 5, compare open red circles with solid black circles). Furthermore, a 1-D setup model [e.g., (1) with $\partial S_{xy}/\partial y = 0$] accurately predicts the alongshore variations in the observed setup (compare Figure 3a with Figure 3b; open red circles in Figure 5), suggesting the observed alongshore variation of setup in the surfzone (Figure 3a) results primarily from alongshore variations of S_{xx} observed at the outer edge of the surfzone (Figure 4a).

4.2. Alongshore Flows: Alongshore Momentum Balance

[21] The effect of alongshore gradients in setup on alongshore flows is examined using the observations and the simplified alongshore momentum balance (6).

4.2.1. Case Study: 27 October 2003

[22] Data from 27 October 2003 (see section 3.1) are used to generate 24-h average curves of $\bar{\eta}$ (e.g., Figure 3a) and S_{yy} (not shown) versus water depth for each cross-shore transect. On the basis of these curves, the alongshore gradients of $\bar{\eta}$ and S_{yy} are estimated using the values measured on neighboring transects and central differencing at the tidally varying depth of the 1.0-m isobath sensors. The cross-shore gradient of S_{xy} is estimated between the sensors on the 2.5- and 1.0-m isobaths and the shoreline (see Appendix), and the average of the two values is used to approximate $\partial S_{xy}/\partial x$ at the depth of the 1.0-m isobath. All terms are estimated only for data records when the 1.0-m isobath sensor was in the surfzone.

[23] Far from the canyon (e.g., $y = 2321$ m), $\partial S_{xy}/\partial x$ usually is the largest term in (6) (Figure 6a). Even though $\partial S_{xy}/\partial x$ is relatively small because the incident wave angles are small (about 5° from normal), the alongshore-gradient terms are even smaller. Near the canyon head (e.g., $y = 1450$ m), where alongshore gradients are expected to be important, $|(\rho g h)\partial\bar{\eta}/\partial y| < |\partial S_{xy}/\partial x|$ for $h > 1.3$ m, but $|(\rho g h)\partial\bar{\eta}/\partial y| > |\partial S_{xy}/\partial x|$ for $h < 1.2$ m (Figure 6b). Setup increases toward the shoreline, allowing for larger alongshore pressure gradients, while $\partial S_{xy}/\partial y$ either remains approximately constant or decreases shoreward owing to wave dissipation and refraction. Thus setup gradients become relatively more important in the middle- and inner-surfzones (the outer surfzone is estimated to be near $h = H_{rms,avg}/0.42$). At all alongshore locations, $\partial S_{yy}/\partial y$ is approximately an order of magnitude smaller than $(\rho g h)\partial\bar{\eta}/\partial y$, and, therefore, is neglected in the analysis below.

[24] Waves at the outer edge of the surfzone on 27 October 2003 were predominately from the south (Figure 2b), creating a negative wave forcing that drives currents (V) toward the north ($V > 0$). For example, far from the canyon head, where the setup-induced pressure gradient is small (Figure 7, green squares), the wave forcing is to the north ($\partial S_{xy}/\partial x < 0$, green circles in Figure 7) and the alongshore current flows northward ($V > 0$). However, near the canyon,

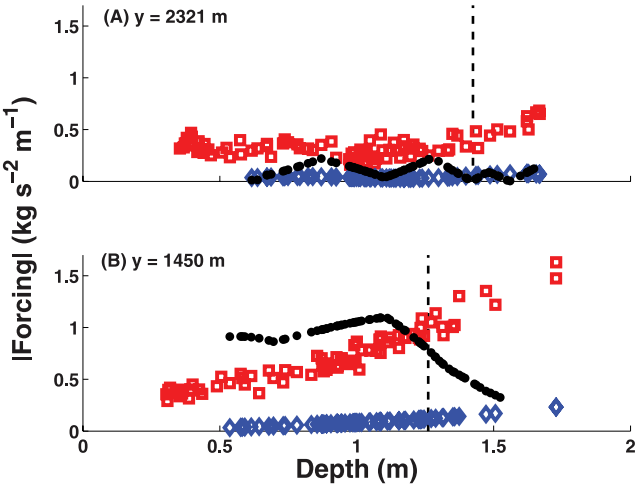

Figure 6. Magnitude of the alongshore forcing owing to alongshore gradients of setup, $[(\rho gh)\partial\bar{\eta}/\partial y$, solid black circles], cross-shore gradients of S_{xy} $[\partial S_{xy}/\partial x$, open red squares], and alongshore gradients of S_{yy} $[\partial S_{yy}/\partial y$, open blue diamonds] versus water depth for (A) y = 2321 m and (B) y = 1450 m using the 85 and 79 8.5-min-long data records from 0:00 to 23:42 27 October 2003 when the 1.0-m isobath sensor was in the surfzone. Vertical dashed lines are $h = H_{rms,avg}/0.42$, where $H_{rms,avg}$ is the average (over all the 8.5-min runs from 27 October) of the root-mean square wave height observed at the 2.5-m depth isobath.

although the wave forcing is to the north (orange pluses in Figure 7), the alongshore current flows southward ($V < 0$), in the direction of the large southward-directed pressure gradients (orange crosses in Figure 7). Comparing the northward flows (V as large as 0.6 m/s) far from the canyon (green symbols in Figure 7) driven by $-0.5 < \partial S_{xy}/\partial x < 0$ kg/(s^2 m) with the southward flows (V as large as -0.7 m/s) near the canyon (orange symbols in Figure 7) driven by a combination of stronger northward wave forcing $[-1.0 < \partial S_{xy}/\partial x < -0.5$ kg/(s^2 m)] and large southward pressure gradients $[(\rho gh)\partial\bar{\eta}/\partial y \approx 1$ kg/(s^2 m)] suggests that the setup-induced pressure gradients observed here can drive flows greater than 1 m/s, and possibly as great as 2 m/s.

[25] Observation-based estimates of the total forcing $\partial S_{xy}/\partial x + (\rho gh)\partial\bar{\eta}/\partial y$ are correlated with $-\rho\langle|\vec{u}|v\rangle$ (r^2 = 0.68, not shown). As expected (Figure 6), including $\partial S_{yy}/\partial y$ in the forcing does not affect the results (r^2 = 0.70). Similar results (r^2 = 0.67) are found if predicted (by the 1-D setup model) $\bar{\eta}$ is used instead of observed $\bar{\eta}$ (i.e., if $\partial\bar{\eta}/\partial y$ is estimated from Figure 3b instead of 3a).

4.2.2. Numerical Model Predictions

[26] The observation-based estimates of the radiation stresses and setup gradients (Figures 6 and 7) are crude because the observations are spatially and temporally (e.g., 24-h averages are required to estimate alongshore gradients) sparse. Therefore the numerical model based on (1) (discussed in 4.1) is used to estimate local forcing terms at 1-m intervals along each shore-normal instrumented transect. The model is applied to all data records when large wave height gradients were observed near the canyon head (defined as the 200 one-hour runs when H_{rms} at y = 1450 m was at least 50% larger than H_{rms} at y = 1300 m), the 1.0-m isobath sensor was in the surfzone, and the bathymetry measured by the GPS-system was within 0.3 m of that measured by altimeters colocated with the current meters (resulting in 50 and 30 1-h runs at y = 2321 and 1450 m, respectively).

[27] The model is driven with hourly (rather than 8.5 min) estimates of the wave characteristics and water depth to reduce small time-scale fluctuations in $\bar{\eta}$. The forcing $\partial S_{xy}/\partial x$ is estimated by finite differencing over a cross-shore distance of 10 m centered on the sensor location, but the results are unchanged if this gradient is estimated over distances between 5 and 40 m. The alongshore gradient in setup, $\partial\bar{\eta}/\partial y$, is found by central differencing the setup predicted along neighboring cross-shore transects. The forcing terms are compared with 1-h averages of the velocity term $-\rho\langle|\vec{u}|v\rangle$ estimated from the observed flows.

[28] Far from the canyon ($1800 < y < 2700$ m, e.g., green symbols in Figure 8), where $\partial\bar{\eta}/\partial y$ is expected to be small [i.e., the right-hand side of (6) is dominated by $\partial S_{xy}/\partial x$], the squared correlation between the total forcing $[\partial S_{xy}/\partial x + (\rho gh)\partial\bar{\eta}/\partial y]$ and the velocity term $[-\rho\langle|\vec{u}|v\rangle]$ (r^2 = 0.75, Figure 8c) is similar to the correlation between the S_{xy}-only forcing and the velocity term (r^2 = 0.78, Figure 8a). The slopes of the least squares fit lines between the forcings and the velocity term [e.g., (6)] imply drag coefficients c_d of 0.0024 and 0.0019 for the total and S_{xy}-only forcing,

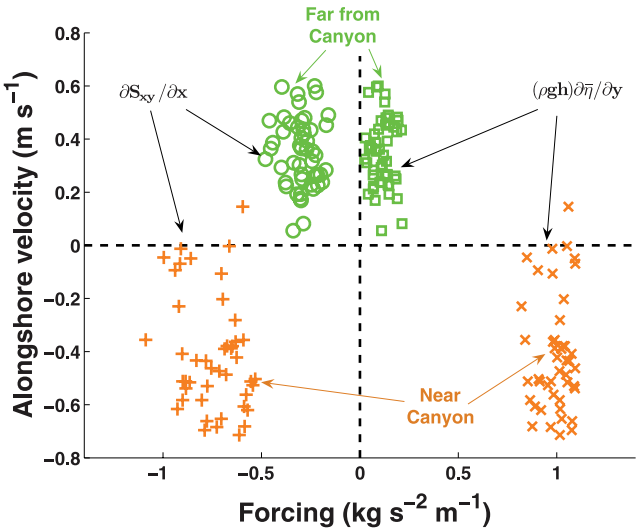

Figure 7. Mean alongshore velocity, V, observed with the 1.0-m isobath sensors versus the forcing [the circles and pluses are $\partial S_{xy}/\partial x$; the squares and crosses are $(\rho gh)\partial\bar{\eta}/\partial y$] at y = 2321 m (green symbols, far from canyon) and y = 1450 m (orange symbols, near canyon) on 27 October 2003. There were 50 (far from canyon) and 45 (near canyon) 8.5-min data records when the 1.0-m isobath sensor was well within the surfzone (shallower than the vertical dashed lines in Figure 6). Both far from and near the canyon, waves approached the shoreline from the south ($\partial S_{xy}/\partial x$ is negative), and the pressure gradients provided an opposing force $[(\rho gh)\partial\bar{\eta}/\partial y$ is positive]. Far from the canyon (green), pressure gradients were weak, and alongshore flows were northward (positive). Near the canyon, pressure gradients dominated, and alongshore flows (with one exception) were southward (negative).

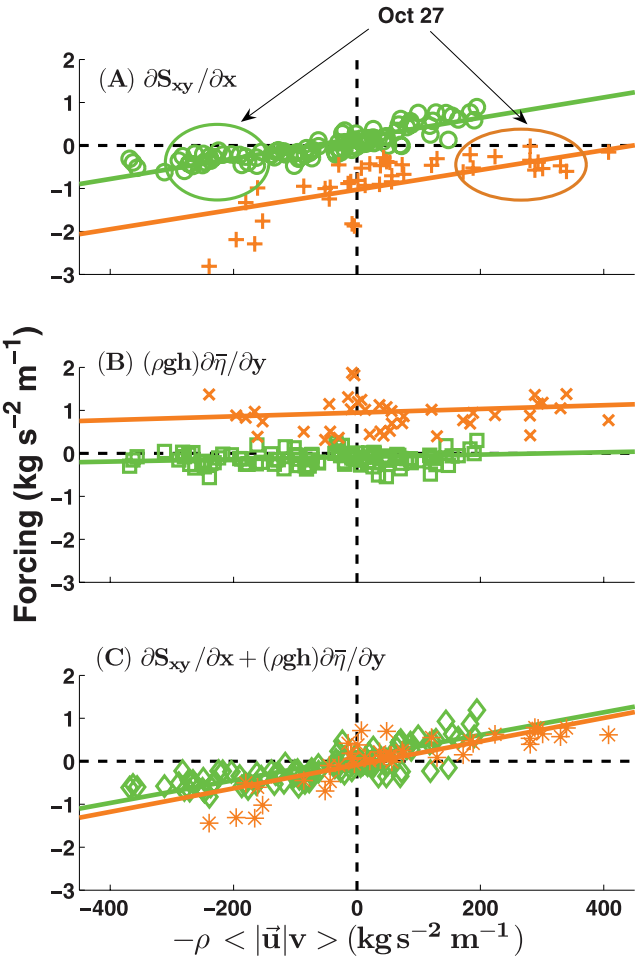

Figure 8. Forcing terms (A) $\partial S_{xy}/\partial x$, (B) $(\rho gh)\partial\bar{\eta}/\partial y$, and (C) the sum $\partial S_{xy}/\partial x + (\rho gh)\partial\bar{\eta}/\partial y$ versus the velocity term $(-\rho\langle|\vec{u}|v\rangle)$ in the bed stress formulation at the 1.0-m isobath sensors far from the canyon (y = 2321 m) (green circles, squares, and diamonds in A, B, and C, respectively) and near the canyon (y = 1450 m) (orange pluses, crosses, and asterisks in A, B, and C, respectively) for all data runs when large gradients in H_{rms} on the 2.5-m isobath were observed for 1300 < y < 1450 m. The solid lines are the least squares fits of the symbols with the same color. The data from 27 October 2003 are highlighted by the ellipses in A.

respectively. Although the setup gradient term, $(\rho gh)\partial\bar{\eta}/\partial y$, is relatively small (Figure 8b, green squares), including it alters c_d by approximately 25%. The c_d values found here are consistent with values from beaches with alongshore-homogeneous waves and bathymetry [*Feddersen et al.*, 1998, 2004; *Ruessink et al.*, 2001], and with values used in numerical simulations of the circulation at this site [*Long and Özkan-Haller*, 2005].

[29] Near the canyon head (1300 < y < 1450 m), $\partial S_{xy}/\partial x$ and $(\rho gh)\partial\bar{\eta}/\partial y$ have similar magnitudes, but opposite signs (compare orange symbols in Figure 8a with those in Figure 8b), and neither term alone can explain the alongshore current direction, which sometimes is toward the north and other times is toward the south. However, the correlation between the total forcing and the velocity term (r^2 = 0.71, Figure 8c, orange asterisks), as well as the corresponding c_d = 0.0025, are similar to values estimated far from the canyon (r^2 = 0.75, c_d = 0.0024). Therefore alongshore gradients in setup must be included to model alongshore flows near the canyon head.

[30] Alongshore gradients in the incident wave height are reduced in the surfzone where waves are depth limited (i.e., $H_{rms} = \gamma h$), and thus gradients in S_{yy} likely will be small along an isobath within the surfzone. Near the canyon (i.e., 1000 < y < 1500 m) where alongshore gradients are expected to be important, $\partial S_{yy}/\partial y$ at the 1.0-m isobath sensors was less than 20% of $(\rho gh)\partial\bar{\eta}/\partial y$ for 90% of the records, and including $\partial S_{yy}/\partial y$ estimated from model predictions (calculated similar to estimates of $\partial\bar{\eta}/\partial y$) changes r^2 and c_d by less than 5%. However, gradients in S_{yy} may be more important on beaches with strong alongshore-bathymetric nonuniformities such as rip channels [*Haller et al.*, 2002].

[31] The sensor array used here can resolve large-scale [O(few-hundred m)] circulation patterns, but not small-scale [O(<100 m)] features that may be caused by unresolved bathymetric variations, or by small-spatial and short-temporal fluctuations in the radiation stresses. For example, rip currents observed with video during the experiment often had length scales of O(100 m) [*Long and Özkan-Haller*, 2005], and thus may contribute to scatter and bias in the simple momentum balance used here.

[32] Order of magnitude estimates based on 1-h averages of the observed currents suggest that one or both of the nonlinear advective terms (neglected here) could be important to the alongshore momentum balance, consistent with previous results [*Putrevu et al.*, 1995; *Haller et al.*, 2002; *Long and Özkan-Haller*, 2005; *Schmidt et al.*, 2005]. Although the nonlinear terms could not be estimated accurately with this data set, their inclusion would not change the conclusion that alongshore pressure gradients contribute significantly to the observed flows.

5. Conclusions

[33] Wave-driven setup observed onshore of large alongshore variations in the incident wave height is predicted well by a one-dimensional model that neglects alongshore gradients in the diagonal component of the wave radiation stress tensor, S_{xy}. The observed alongshore variations in setup resulted primarily from alongshore variations in the wave radiation stress component S_{xx} at the outer edge of the surfzone.

[34] For data records when alongshore gradients in the incident wavefield were large, momentum balances that neglect setup gradients often predict surfzone currents flowing opposite those observed. When setup gradients are included, the direction (and magnitude) of the alongshore flow is predicted correctly, demonstrating that setup-induced pressure gradients caused by an inhomogeneous incident wavefield can drive significant alongshore currents.

Appendix A: Estimates of Radiation Stress Gradients

[35] Cross-shore gradients are estimated from the observed and predicted radiation stresses along each shore-normal transect. Alongshore gradients are estimated along isobaths (in the direction perpendicular to the shore-normal transect)

and by using central differencing for data between $1000 < y < 2700$ m, and backwards and forwards differencing at the northern and southern ends of the sensor array, respectively. The conclusions are not changed if ∂y is estimated as the alongshore distance between transects ($\partial y = y_1 - y_2$), or the magnitude of the vector distance between the transects $\left[\partial y = \sqrt{(y_2 - y_1)^2 + (x_2 - x_2)^2}\right]$.

[36] The components of the wave radiation stress tensor (S_{xx}, S_{xy}, and S_{yy}) are calculated using wave angles, θ, relative to local shore normal at each cross-shore transect. The shoreline is not straight (Figure 1a), and the orientation of shore normal varied by up to 7° between neighboring transects. These rotations could cause $\partial S_{xy}/\partial y$ to be underestimated by about 50% and $\partial S_{yy}/\partial y$ to be overestimated by about 7%. However, the relative importance of $\partial S_{xy}/\partial y$ and $\partial S_{xx}/\partial x$ to wave-driven setup, and of $\partial S_{xy}/\partial x$, $\partial \eta/\partial y$, and $\partial S_{yy}/\partial y$ to alongshore flows is not sensitive to rotation of shore normal within this range.

[37] The observation-based, surfzone-averaged cross-shore gradients of S_{xx} (section 4.1) and S_{xy} (section 4.2.1, Figures 6 and 7) are estimated by using the measurements from the sensors on both the 2.5- and 1.0-m isobaths, and by assuming that S_{xx} and S_{xy} are 0 at the shoreline (defined as the location where the still water level intersects the measured sand level). The cross-shore distance ∂x is estimated as the distance between the shoreline and either the sensor location (if the sensor is in the surfzone) or the outer edge of the surfzone (defined as the most seaward location where $h = H_{rms}/\gamma$, with $\gamma = 0.42$) (if the sensor is seaward of the surfzone). The conclusions are not changed if values of $\gamma = 0.32$, 0.52, or 0.62 are used.

[38] The observation-based, alongshore gradients of S_{xy} (section 4.1), S_{yy}, and η (section 4.2.1, Figures 6 and 7) are estimated for each data record along both the 2.5- and 1.0-m isobaths. The more than 2-m tidal change with respect to mean sea level provides a range of water depths at each isobath.

[39] The ratio of the observation-based estimates of $\partial S_{xy}/\partial y$ to $\partial S_{xx}/\partial x$ is less than 0.1 on all cross-shore transects, suggesting that the contribution to setup from $\partial S_{xy}/\partial y$ is small for these observations. When a sensor was located seaward of the surfzone, S_{xx} was assumed to be constant between the sensor and the outer edge of the surfzone. Thus the effects of wave shoaling and refraction between the sensor location and the outer edge of the surfzone were neglected in the observation-based estimates. Shoaling increases the wave energy E_w and refraction decreases θ, resulting in an increase to S_{xx}. However, S_{xy} remains constant, because increases in E_w and $\cos(\theta)$ are canceled by decreases in c_g (conservation of energy flux requires $E_w c_g \cos(\theta) =$ constant), and decreases in $\sin(\theta)$ are canceled by decreases in c (Snell's law requires $\sin(\theta)/c =$ constant). Therefore neglecting wave shoaling and refraction will not change the conclusion that the contribution to setup of $\partial S_{xy}/\partial y$ is small relative to the contribution of $\partial S_{xx}/\partial x$.

[40] **Acknowledgments.** Staff from the PVLAB (Woods Hole Oceanographic Institution) and the Center for Coastal Studies (Scripps Institution of Oceanography) are thanked for their efforts in obtaining the observations. The reviewers are thanked for their insightful comments and suggestions. Funding was provided by the Office of Naval Research and the National Science Foundation.

References

Apotsos, A., B. Raubenheimer, S. Elgar, R. T. Guza, and J. A. Smith (2006), A note on setup sensitivity and prediction accuracy, *Proc. 30th Int. Conf. Coastal Eng.*, *1*, 946–958.

Apotsos, A., B. Raubenheimer, S. Elgar, R. T. Guza, and J. A. Smith (2007), Effects of wave rollers and bottom stress on wave setup, *J. Geophys. Res.*, *112*(C2), C02003, doi:10.1029/2006JC003549.

Apotsos, A., B. Raubenheimer, S. Elgar, and R. T. Guza (2008), Testing and calibrating parametric wave transformation models on natural beaches, *Coastal Eng.*, *55*(3), 224–235.

Battjes, J. A., and M. J. F. Stive (1985), Calibration and verification of a dissipation model for random breaking waves, *J. Geophys. Res.*, *90*(C5), 9159–9167.

Chen, Q., J. T. Kirby, R. A. Dalrymple, F. Shi, and E. B. Thornton (2003), Boussinesq modeling of longshore currents, *J. Geophys. Res.*, *108*(C11), 3362, doi:10.1029/2002JC001308.

Elgar, S., T. H. C. Herbers, and R. T. Guza (1994), Reflection of ocean surface gravity waves from a natural beach, *J. Phys. Oceanogr.*, *24*, 1503–1511.

Feddersen, F. (2004), Effect of wave directional spread on the radiation stress: Comparing theory and observations, *Coastal Eng.*, *51*, 473–481.

Feddersen, F., R. T. Guza, and S. Elgar (2004), Inverse modeling of the one-dimensional setup and alongshore current in the nearshore, *J. Phys. Oceangr.*, *34*, 920–933.

Feddersen, F., R. T. Guza, S. Elgar, and T. H. C. Herbers (1998), Alongshore momentum balances in the nearshore, *J. Geophys. Res.*, *103*(C8), 15,667–15,676.

Haas, K. A., I. A. Svendsen, M. C. Haller, and Q. Zhao (2003), Quasi-three-dimensional modeling of rip current systems, *J. Geophys. Res.*, *108*(C7), 3217, doi:10.1029/2002JC001355.

Haller, M. C., R. A. Dalrymple, and I. A. Svendsen (2002), Experimental study of nearshore dynamics on a barred beach with rip channels, *J. Geophys. Res.*, *107*(C6), 3061, doi:10.1029/2001JC000955.

Herbers, T. H. C., and R. T. Guza (1990), Estimation of directional wave spectra from multicomponent observations, *J. Phys. Oceanogr.*, *20*, 1703–1724.

Kuik, A., G. van Vledder, and L. Holthuijsen (1988), A method for routine analysis of pitch-and-roll buoy data, *J. Phys. Oceanogr.*, *18*, 1020–1034.

Lentz, S., and B. Raubenheimer (1999), Field observations of wave setup, *J. Geophys. Res.*, *104*(C11), 25,867–25,875.

Lentz, S., R. T. Guza, S. Elgar, F. Feddersen, and T. H. C. Herbers (1999), Momentum balances on the North Carolina inner shelf, *J. Geophys. Res.*, *104*(C8), 18,205–18,226.

Long, J. W., and H. T. Özkan-Haller (2005), Offshore controls on nearshore rip currents, *J. Geophys. Res.*, *110*, C12007, doi:10.1029/2005JC003018.

Longuet-Higgins, M. S. (1970), Longshore currents generated by obliquely incident sea waves, *J. Geophys. Res.*, *75*(33), 6778–6789.

Longuet-Higgins, M. S., and R. W. Stewart (1962), Radiation stress and mass transport in gravity waves, with application to 'surf-beats', *J. Fluid Mech.*, *13*, 481–504.

Longuet-Higgins, M. S., and R. W. Stewart (1964), Radiation stresses in water waves: A physical discussion with applications, *Deep Sea Res.*, *11*, 529–562.

Magne, R., K. A. Belibassakis, T. H. C. Herbers, F. Ardhuin, W. C. O'Reilly, and V. Rey (2007), Evolution of surface gravity waves over a submarine canyon, *J. Geophys. Res.*, *112*(C1), C01002, doi:10.1029/2005JC003035.

Mei, C. C. (1989), *The Applied Dynamics of Ocean Surface Waves*, World Sci., River Edge, NJ.

Özkan-Haller, H. T., and J. T. Kirby (1999), Nonlinear evolution of shear instabilities of the longshore current: A comparison of observations and computations, *J. Geophys. Res.*, *104*(C11), 25,953–25,984.

Putrevu, U., J. Oltman-Shay, and I. A. Svendsen (1995), Effect of alongshore nonuniformities on longshore current predictions, *J. Geophys. Res.*, *100*(C8), 16,119–16,130.

Raubenheimer, B., S. Elgar, and R. T. Guza (1998), Estimating wave heights from pressure measured in sand bed, *J. Waterw. Port Coastal Ocean Eng.*, 151–154.

Raubenheimer, B., R. T. Guza, and S. Elgar (2001), Field observations of wave-driven setdown and setup, *J. Geophys. Res.*, *106*(C3), 4629–4638.

Reniers, A. J. H. M., and J. A. Battjes (1997), A laboratory study of longshore currents over barred and non-barred beaches, *Coastal Eng.*, *30*, 1–22.

Reniers, A. J. H. M., A. R. Van Dongeren, J. A. Battjes, and E. B. Thornton (2002), Linear modeling of infragravity waves during Delilah, *J. Geophys. Res.*, *107*(C10), 3137, doi:10.1029/2001JC001083.

Ruessink, B. G., J. R. Miles, F. Feddersen, R. T. Guza, and S. Elgar (2001), Modeling the alongshore current on barred beaches, *J. Geophys. Res.*, *106*(C10), 22,451–22,463.

Schmidt, W. E., R. T. Guza, and D. N. Slinn (2005), Surf zone currents over irregular bathymetry: Drifter observations and numerical simulations, *J. Geophys. Res.*, *110*, C12015, doi:10.1029/2004JC002421.

Slinn, D. N., J. S. Allen, and R. A. Holman (2000), Alongshore currents over variable beach topography, *J. Geophys. Res.*, *105*(C7), 16,971–16,998.

Stive, M. J. F., and H. J. De Vriend (1994), Shear stress and mean flow in shoaling and breaking waves, *Proc. 24th Int. Conf. Coastal Eng.*, 594–608.

Svendsen, I. A. (1984a), Wave heights and set-up in a surf zone, *Coastal Eng.*, *8*, 303–329.

Svendsen, I. A. (1984b), Mass flux and undertow in a surf zone, *Coastal Eng.*, *8*, 347–365.

Thomson, J., S. Elgar, B. Raubenheimer, T. H. C. Herbers, and R. T. Guza (2006), Tidal modulation of infragravity waves via nonlinear energy losses in the surfzone, *Geophys. Res. Lett.*, *33*, L05601, doi:10.1029/2005GL025514.

Thomson, J., S. Elgar, T. H. C. Herbers, B. Raubenheimer, and R. T. Guza (2007), Refraction and reflection of infragravity waves near submarine canyons, *J. Geophys. Res.*, *112*, C10009, doi:10.1029/2007JC004227.

Thornton, E. B., and R. T. Guza (1983), Transformation of wave height distribution, *J. Geophys. Res.*, *88*(C10), 5925–5938.

Van Dongeren, A., A. Reniers, J. Battjes, and I. Svendsen (2003), Numerical modeling of infragravity wave response during DELILAH, *J. Geophys. Res.*, *108*(C9), 3288, doi:10.1029/2002JC001332.

A. Apotsos, S. Elgar, and B. Raubenheimer, Woods Hole Oceanographic Institution, Applied Ocean Physics and Engineering, MS 9, Woods Hole, MA 02543, USA. (aapotsos@whoi.edu)

R. T. Guza, Scripps Institution of Oceanography, Integrative Oceanography Division, University of California at San Diego, La Jolla, CA 92093-0209, USA.